Chao-Yang Song
Engineering Product Development Pillar,
Singapore University of Technology and Design,
20 Dover Drive,
Singapore 138682, Singapore
e-mail: chaoyang_song@sutd.edu.sg

Yan Chen[1]
Professor
Key Laboratory of Mechanism
Theory and Equipment Design of
Ministry of Education,
School of Mechanical Engineering,
Tianjin University,
Tianjin 300072, China
e-mail: yan_chen@tju.edu.cn

I-Ming Chen
Associate Professor
School of Mechanical and
Aerospace Engineering,
Nanyang Technological University,
50 Nanyang Avenue,
Singapore 639798, Singapore
e-mail: michen@ntu.edu.sg

Kinematic Study of the Original and Revised General Line-Symmetric Bricard 6*R* Linkages

In this paper, the solutions to closure equations of the original general line-symmetric Bricard 6R linkage are derived through matrix method. Two independent linkage closures are found in the original general line-symmetric Bricard 6R linkage, which are line-symmetric in geometry conditions, kinematic variables and spatial configurations. The revised general line-symmetric Bricard 6R linkage differs from the original linkage with negatively equaled offsets on the opposite joints. Further analysis shows that the revised linkage is equivalent to the original linkage with different setups on joint axis directions. As a special case of the general line-symmetric Bricard linkage, the line-symmetric octahedral Bricard linkage also has two forms in the closure equations. Their closure curves are not independent but joined into a full circle. This work offers an in-depth understanding about the kinematics of the general line-symmetric Bricard linkages.
[DOI: 10.1115/1.4026339]

Keywords: kinematics, the Bricard linkage, closure equations, multiple closures

1 Introduction

The Bricard linkages comprise three deformable octahedrons: the line-symmetric octahedral case, the plane-symmetric octahedral case, and the doubly collapsible octahedral case [1]; and three spatial linkages: the general line-symmetric case, the general plane-symmetric case, and the trihedral case [2]. Bricard later pointed out that the line-symmetric octahedral case is a special case of the general line-symmetric linkage case [2,3]. Baker studied all cases of Bricard linkages systematically and derived their closure equations [3]. Later, Phillips reviewed the Bricard linkages and their relationship with other overconstrained linkages [4,5].

The octahedral cases of Bricard linkages attracted a number of kinematic studies. A comprehensive analysis to the three octahedral cases was done by Bennett [6]. Baker noticed the relationship of a special line-symmetric octahedral Bricard linkage in stationary and linkage configurations with respect to the conformation of cyclohexane molecular in chair and boat forms [7]. The closure equations of the three octahedral cases of Bricard linkages were derived analytically using matrix transformation method by Lee [8]. Recently, Chai and Chen found out that the line-symmetric octahedral Bricard linkage with identical twists and offsets always has a stationary structural configuration, which is independent of its mobile linkage form [9]. In engineering applications, the octahedral cases of Bricard linkages are related to parallel manipulators, such as the Stewart–Gough manipulator [10–12] and triangular symmetric simplified manipulators [13,14], which are widely used as flight simulators and milling machines. The independent work by Nelson demonstrated the possibility of building large network of polyhedral with the octahedral cases of Bricard linkages [15].

As for the three linkage cases, a plate-form model of the trihedral Bricard 6*R* linkage was made and analyzed by Goldberg [16]. Yu [17] studied the geometry of the trihedral case with respect to its circumscribed sphere and associated hyperboloid. Wohlhart's early work [18] showed that there are two distinct trihedral cases of Bricard linkages. Due to the special geometry constraint of the Bricard linkages, the reciprocal screw system is extensively used for analysis of such mechanisms. Using the reciprocal screw system, it was found that for any configuration of the general line-symmetric Bricard linkage, the central axis of the linear complex defined by the joint axis is orthogonally intersected to the linkage's line of symmetry [19]. The reciprocal screw system of the general plane-symmetric six-screw linkage was also analyzed by Baker [20], which covers the plane-symmetric case of Bricard linkages. Based on the direct elimination method with optimization theory, Lee [21] proposed a numerical scheme to solve the reciprocal screw system of the Bricard linkages, which gives the necessary solutions to a given linkage, and it is not sufficient to present all possible solutions. Recently, a threefold-symmetric Bricard linkage was proposed to explore the application of Bricard linkage for the design of deployable structures [22]. A special line-symmetric and plane-symmetric Bricard linkages were analyzed with regards to its unique bifurcation behaviours [23]. Further attempt was made to find and identify possible solutions of spatial 6*R* mechanism with three adjacent parallel axes [24], and the research on the Wohlhart's symmetric mechanism [25], which is usually identified as the Wohlhart's hybrid 6*R* linkage [26,27], explores the industrial application of this linkage as a translator.

To conduct the kinematic study of the general line-symmetric Bricard linkage, the D-H parameters [28] in Fig. 1 are commonly adopted and a homogeneous transformation matrix could be assembled as

$$\mathbf{T}_{i(i+1)} = \begin{bmatrix} \mathbf{R}_{3\times3} & \mathbf{d}_{3\times1} \\ \mathbf{0}_{1\times3} & 1 \end{bmatrix} = \begin{bmatrix} \cos\theta_i & -\cos\alpha_{i(i+1)}\sin\theta_i & \sin\alpha_{i(i+1)}\sin\theta_i & a_{i(i+1)}\cos\theta_i \\ \sin\theta_i & \cos\alpha_{i(i+1)}\cos\theta_i & -\sin\alpha_{i(i+1)}\cos\theta_i & a_{i(i+1)}\sin\theta_i \\ 0 & \sin\alpha_{i(i+1)} & \cos\alpha_{i(i+1)} & R_i \\ 0 & 0 & 0 & 1 \end{bmatrix} \quad (1)$$

[1]Corresponding author.

Contributed by the Mechanisms and Robotics Committee of ASME for publication in the Journal of Mechanisms and Robotics. Manuscript received March 21, 2013; final manuscript received October 17, 2013; published online April 3, 2014. Assoc. Editor: Philippe Wenger.

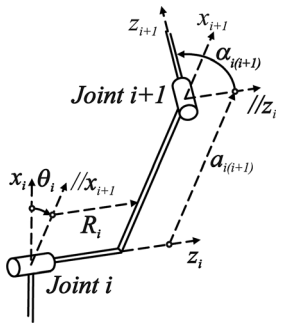

Fig. 1 The setup of the Denavit and Hartenberg's parameters

The geometry conditions of the *original* general line-symmetric Bricard linkage are

$$\begin{aligned} &a_{12}=a_{45}, \quad a_{23}=a_{56}, \quad a_{34}=a_{61} \\ &\alpha_{12}=\alpha_{45}, \quad \alpha_{23}=\alpha_{56}, \quad \alpha_{34}=\alpha_{61} \\ &R_1=R_4, \quad R_2=R_5, \quad R_3=R_6 \end{aligned} \tag{2}$$

Although the closure equations of the general line-symmetric Bricard linkage have been derived by Baker [3], it requires more elaborations about these equations for a better understanding. Due to the line-symmetric geometry, the revolute variables of the original line-symmetric Bricard linkage are positively equaled on the opposite joints as $\theta_1=\theta_4$, $\theta_2=\theta_5$, and $\theta_3=\theta_6$ [3]. Yet, a numerical search of new and revised overconstrained linkages was conducted by Mavroidis and Roth [29], where a *revised* closure of the general line-symmetric Bricard linkage was found with negatively equaled offsets on the opposite joints as below:

$$\begin{aligned} &a'_{12}=a'_{45}, \quad a'_{23}=a'_{56}, \quad a'_{34}=a'_{61}, \\ &\alpha'_{12}=\alpha'_{45}, \quad \alpha'_{23}=\alpha'_{56}, \quad a'_{34}=\alpha'_{61}, \\ &R'_1=-R'_4, \quad R'_2=-R'_5, \quad R'_3=-R'_6 \end{aligned} \tag{3}$$

It was obtained from numerical method that the revolute variables in the revised general line-symmetric Bricard linkage are negatively equaled on the opposite joints as $\theta'_1=-\theta'_4$, $\theta'_2=-\theta'_5$, and $\theta'_3=-\theta'_6$ [29]. Despite the similar relationship in geometry conditions and kinematic variables, the original and revised line-symmetric Bricard linkages are usually considered as two distinct linkages.

The original line-symmetric Bricard linkage is with perfect line-symmetry property in both geometric parameters and kinematic variables, while the revised one is without line-symmetry property in both aspects, but exhibits a line-symmetric configuration in the full-cycle motion. Therefore, the focus of this paper is to study the kinematics of the general line-symmetric Bricard linkage and to explore the relationship between the *original* and *revised* general line-symmetric Bricard linkages. When deriving the closure equations, only the relationship among the geometric parameters is taken into account. However, the relationship among the kinematic variables is not considered initially. Instead, it will be the conclusion derived from the closure equations. The layout of this paper is as follows. The solutions of closure equations of the original and revised linkages are derived in Secs. 2 and 3, respectively. Section 4 discusses the relationship between the original and revised linkages. Conclusion and further discussions are drawn in Sec. 5, which ends the paper.

2 The Solutions of Closure Equations of the Original General Line-Symmetric Bricard Linkage

The simplified geometry conditions of the original general line-symmetric Bricard linkage are

$$a_{i(i+1)}=a_{(i+3)(i+4)}, \quad \alpha_{i(i+1)}=\alpha_{(i+3)(i+4)}, \quad R_i=R_{(i+3)} (i=1,2,3) \tag{4}$$

Note that to ensure this is a close-loop 6*R* mechanism, the subscripts must be the remainder of 6 in positive numbers. The closure condition is

$$\mathbf{T}_{12}\mathbf{T}_{23}\cdots\mathbf{T}_{61}=\mathbf{I} \tag{5}$$

which could be represented as

$$\mathbf{T}_{i(i+1)}\mathbf{T}_{(i+1)(i+2)}\mathbf{T}_{(i+2)(i+3)}=\mathbf{T}^{-1}_{(i+5)(i+6)}\mathbf{T}^{-1}_{(i+4)(i+5)}\mathbf{T}^{-1}_{(i+3)(i+4)} \tag{6}$$

In the transformation matrix in Eq. (1), the angular parameters, including twist and revolute variable, are stored in both rotational matrix $\mathbf{R}_{3\times3}$ and translational vector $\mathbf{d}_{3\times1}$. The length parameters, including link length and offset, are only stored in the translational vector $\mathbf{d}_{3\times1}$. In Eq. (6), we may first use the rotational matrix $\mathbf{R}_{3\times3}$ to derive the relationship among the angular parameters, and then introduce the length parameters using the translational vector $\mathbf{d}_{3\times1}$ to derive the solutions of closure equations. Here, the entry (1, 1) in Eq. (6) is extracted and reformed as

$$\begin{aligned} &\begin{pmatrix} \cos\theta_i\cos\theta_{i+1}\cos\theta_{i+2} \\ -\cos\theta_{i+3}\cos\theta_{i+4}\cos\theta_{i+5} \end{pmatrix} \\ &-\begin{pmatrix} \sin\theta_i\sin\theta_{i+1}\cos\theta_{i+2} \\ -\sin\theta_{i+3}\sin\theta_{i+4}\cos\theta_{i+5} \end{pmatrix}\cos\alpha_{i(i+1)} \\ &-\begin{pmatrix} \cos\theta_i\sin\theta_{i+1}\sin\theta_{i+2} \\ -\cos\theta_{i+3}\sin\theta_{i+4}\sin\theta_{i+5} \end{pmatrix}\cos\alpha_{(i+1)(i+2)} \\ &+\begin{pmatrix} \sin\theta_i\sin\theta_{i+2} \\ -\sin\theta_{i+3}\sin\theta_{i+5} \end{pmatrix}\sin\alpha_{i(i+1)}\sin\alpha_{(i+1)(1+2)} \\ &-\begin{pmatrix} \sin\theta_i\cos\theta_{i+1}\sin\theta_{i+2} \\ -\sin\theta_{i+3}\cos\theta_{i+4}\sin\theta_{i+5} \end{pmatrix}\cos\alpha_{i(i+1)}\cos\alpha_{(i+1)(i+2)}=0 \end{aligned} \tag{7}$$

Equation (7) must always hold no matter what the values of twist angles are. Thus, one nontrivial solution is when the items in every bracket of Eq. (7) are zero, i.e.,

$$\cos\theta_i\cos\theta_{i+1}\cos\theta_{i+2}-\cos\theta_{i+3}\cos\theta_{i+4}\cos\theta_{i+5}=0 \tag{8a}$$

$$\sin\theta_i\sin\theta_{i+1}\cos\theta_{i+2}-\sin\theta_{i+3}\sin\theta_{i+4}\cos\theta_{i+5}=0 \tag{8b}$$

$$\cos\theta_i\sin\theta_{i+1}\sin\theta_{i+2}-\cos\theta_{i+3}\sin\theta_{i+4}\sin\theta_{i+5}=0 \tag{8c}$$

$$\sin\theta_i\sin\theta_{i+2}-\sin\theta_{i+3}\sin\theta_{i+5}=0 \tag{8d}$$

$$\sin\theta_i\cos\theta_{i+1}\sin\theta_{i+2}-\sin\theta_{i+3}\cos\theta_{i+4}\sin\theta_{i+5}=0 \tag{8e}$$

Substituting Eq. (8*d*) into Eq. (8*e*) gives

$$\cos\theta_{i+1}=\cos\theta_{i+4} \tag{9}$$

From Eq. (8*d*), we have

$$\frac{\sin\theta_i}{\sin\theta_{i+3}}=\frac{\sin\theta_{i+5}}{\sin\theta_{i+2}} \tag{10}$$

By substituting $i = 1, 2, 3$ into Eqs. (9) and (10), we have

$$\cos\theta_2 = \cos\theta_5, \quad \cos\theta_3 = \cos\theta_6, \quad \cos\theta_4 = \cos\theta_1 \tag{11}$$

and

$$\frac{\sin\theta_1}{\sin\theta_4} = \frac{\sin\theta_6}{\sin\theta_3} = \frac{\sin\theta_5}{\sin\theta_2} \tag{12}$$

Considering the domain of definition that $\theta_i \in [-\pi, \pi)$ and Eqs. (8*a*)–(8*c*), the following relationships can be obtained from Eqs. (11) and (12):

$$\text{positive relationship}, \quad \theta_i = \theta_{i+3} \tag{13a}$$

$$\text{negative relationship}, \quad \theta_i = -\theta_{i+3} \tag{13b}$$

In the above process, entry (1, 1) of the transformation matrix in Eq. (6) is selected for the derivation of the relationships shown as Eq. (13). Alternatively, we can also use entries (2, 2) and (3, 3) in Eq. (6) to derive the same relationships in Eq. (13). Note that these entries are all located in the rotational matrix, which contains only the rotational information during coordinate transformation of the links and joints.

Then, the link length and offset located in the translational vector can be considered to derive the solutions of closure equations. Among the simplified expressions of the translational vectors shown in Eq. (14), entry (3, 4) consists of the least unknown variables

$$\mathbf{d}_1 = \mathbf{T}_{(1,4)}(\theta_i, \theta_{i+1}, \theta_{i+2}, \theta_{i+4}, \theta_{i+5}) = 0 \tag{14a}$$

$$\mathbf{d}_2 = \mathbf{T}_{(2,4)}(\theta_i, \theta_{i+1}, \theta_{i+2}, \theta_{i+4}, \theta_{i+5}) = 0 \tag{14b}$$

$$\mathbf{d}_3 = \mathbf{T}_{(3,4)}(\theta_{i+1}, \theta_{i+2}, \theta_{i+4}, \theta_{i+5}) = 0 \tag{14c}$$

By substituting the relationship in Eq. (13) into Eq. (14*c*), for different subscript numbers, we have that

- when $i = 1$, the relationship between θ_2 and θ_3 can be derived
- when $i = 2$, the relationship between θ_1 and θ_3 can be derived
- when $i = 3$, the relationship between θ_1 and θ_2 can be derived

To form the closure equations, θ_1 is taken as the input. Then, only the relationship between θ_1 and $\theta_{2,3}$ will be obtained in the following process. Together with Eq. (13), the complete set of solutions to the closure equations for the original general line-symmetric Bricard 6*R* linkage will be obtained.

2.1 Positive Relationship: $\theta_i = \theta_{i+3}$. Firstly, we consider the case of positive relationship in Eq. (13*a*) that $\theta_i = \theta_{i+3}$, where the revolute variables follow the property of line-symmetry. When $i = 3$, substituting Eq. (13*a*) into Eq. (14*c*) gives

$$\begin{aligned}
&(a_{12}\sin\alpha_{34} + a_{34}\sin\alpha_{12}\cos\alpha_{23})\sin\theta_1 \\
&\quad - (R_2\sin\alpha_{12}\sin\alpha_{34} + R_3\sin\alpha_{12}\cos\alpha_{23}\sin\alpha_{34})\cos\theta_1 \\
&\quad + (a_{12}\sin\alpha_{23} + a_{23}\cos\alpha_{34}\sin\alpha_{12})\sin\theta_2 \\
&\quad - (R_1\sin\alpha_{12}\sin\alpha_{23} + R_3\sin\alpha_{12}\sin\alpha_{23}\cos\alpha_{34})\cos\theta_2 \\
&\quad + R_3\sin\alpha_{23}\sin\alpha_{34}\sin\theta_1\sin\theta_2 \\
&\quad + (a_{34}\cos\alpha_{12}\sin\alpha_{23} + a_{23}\sin\alpha_{34})\sin\theta_1\cos\theta_2 \\
&\quad + (a_{23}\cos\alpha_{12}\sin\alpha_{34} + a_{34}\sin\alpha_{23})\cos\theta_1\sin\theta_2 \\
&\quad - R_3\cos\alpha_{12}\sin\alpha_{23}\sin\alpha_{34}\cos\theta_1\cos\theta_2 \\
&\quad + R_1(\cos\alpha_{12}\cos\alpha_{23} + \cos\alpha_{34}) \\
&\quad + R_2(\cos\alpha_{23}\cos\alpha_{12}\cos\alpha_{34}) \\
&\quad + R_3(1 + \cos\alpha_{12}\cos\alpha_{23}\cos\alpha_{34}) = 0
\end{aligned} \tag{15}$$

The above equation can be simplified as

$$\begin{aligned}
&A_2\sin\theta_1 + B_2\cos\theta_1 + C_2\sin\theta_2 + D_2\cos\theta_2 \\
&\quad + E_2\sin\theta_1\sin\theta_2 + F_2\sin\theta_1\cos\theta_2 + G_2\cos\theta_1\sin\theta_2 \\
&\quad + H_2\cos\theta_1\cos\theta_2 + L_2 = 0
\end{aligned} \tag{16}$$

in which

$$\begin{cases}
A_2 = +(a_{12}\sin\alpha_{34} + a_{34}\sin\alpha_{12}\cos\alpha_{23}) \\
B_2 = -(R_2\sin\alpha_{12}\sin\alpha_{34} + R_3\sin\alpha_{12}\cos\alpha_{23}\sin\alpha_{34}) \\
C_2 = +(a_{12}\sin\alpha_{23} + a_{23}\cos\alpha_{34}\sin\alpha_{12}) \\
D_2 = -(R_1\sin\alpha_{12}\sin\alpha_{23} + R_3\sin\alpha_{12}\sin\alpha_{23}\cos\alpha_{34}) \\
E_2 = +R_3\sin\alpha_{23}\sin\alpha_{34} \\
F_2 = +(a_{34}\cos\alpha_{12}\sin\alpha_{23} + a_{23}\sin\alpha_{34}) \\
G_2 = +(a_{23}\cos\alpha_{12}\sin\alpha_{34} + a_{34}\sin\alpha_{23}) \\
H_2 = -R_3\cos\alpha_{12}\sin\alpha_{23}\sin\alpha_{34} \\
I_2 = +R_1(\cos\alpha_{12}\cos\alpha_{23} + \cos\alpha_{34}) \\
\qquad + R_2(\cos\alpha_{23} + \cos\alpha_{12}\cos\alpha_{34}) \\
\qquad + R_3(1 + \cos\alpha_{12}\cos\alpha_{23}\cos\alpha_{34})
\end{cases} \tag{17}$$

After the tangent half-angle substitution of $\sin\theta_2$ and $\cos\theta_2$, Eq. (16) can be rewritten into

$$\begin{aligned}
&\begin{bmatrix} (A_2\sin\theta_1 + B_2\cos\theta_1 + L_2) \\ -(D_2 + F_2\sin\theta_1 + H_2\cos\theta_1) \end{bmatrix}\tan^2\frac{\theta_2}{2} \\
&\quad + 2(C_2 + E_2\sin\theta_1 + G_2\cos\theta_1)\tan\frac{\theta_2}{2} \\
&\quad + \begin{bmatrix} (A_2\sin\theta_1 + B_2\cos\theta_1 + L_2) \\ +(D_2 + F_2\sin\theta_1 + H_2\cos\theta_1) \end{bmatrix} = 0
\end{aligned} \tag{18}$$

Again, Eq. (18) can be further simplified as

$$Aterm_2 \cdot \tan^2\frac{\theta_2}{2} + Bterm_2 \cdot \tan^2\frac{\theta_2}{2} + Cterm_2 = 0 \tag{19}$$

in which θ_1 is represented in

$$\begin{cases}
Aterm_2 = (A_2\sin\theta_1 + B_2\cos\theta_1 + L_2) \\
\qquad\qquad -(D_2 + F_2\sin\theta_1 + H_2\cos\theta_1) \\
Bterm_2 = 2(C_2 + E_2\sin\theta_1 + G_2\cos\theta_1) \\
Cterm_2 = (A_2\sin\theta_1 + B_2\cos\theta_1 + L_2) \\
\qquad\qquad +(D_2 + F_2\sin\theta_1 + H_2\cos\theta_1)
\end{cases} \tag{20}$$

Solutions to Eq. (19) are

$$\tan\frac{\theta_2}{2} = \frac{-Bterm_2 \pm \sqrt{Bterm_2^2 - 4Aterm_2 \cdot Cterm_2}}{2Aterm_2} \tag{21}$$

in which all symbols are defined in Eqs. (17) and (20). The closure relationship between θ_1 and θ_2 is therefore obtained. Similarly, by analysing Eqs. (13*a*) and (14*c*) with $i = 2$, the relationship between θ_1 and θ_3 can be derived as

$$\tan\frac{\theta_3}{2} = \frac{-Bterm_3 \pm \sqrt{Bterm_3^2 - 4Aterm_3 \cdot Cterm_3}}{2Aterm_3} \tag{22}$$

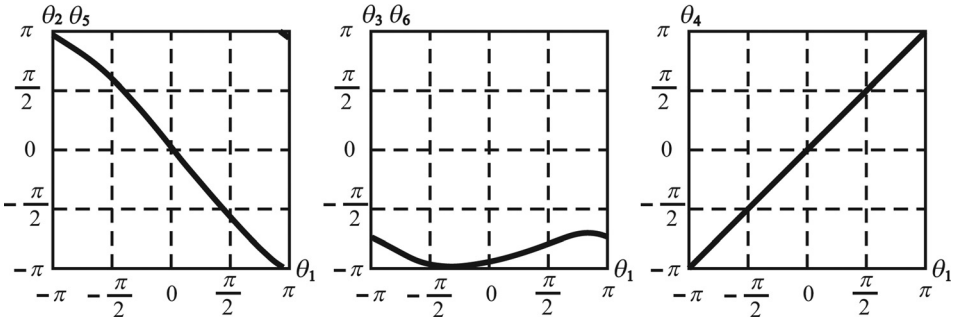

Fig. 2 The kinematic paths of the original Form I general line-symmetric Bricard 6*R* linkage

where

$$\begin{cases} Aterm_3 = (A_3 \sin\theta_1 + B_3 \cos\theta_1 + L_3) \\ \qquad\qquad -(D_3 + F_3 \sin\theta_1 + H_3 \cos\theta_1) \\ Bterm_3 = 2(C_3 + E_3 \sin\theta_1 + G_3 \cos\theta_1) \\ Cterm_3 = (A_3 \sin\theta_1 + B_3 \cos\theta_1 + L_3) \\ \qquad\qquad +(D_3 + F_3 \sin\theta_1 + H_3 \cos\theta_1) \end{cases} \tag{23}$$

and

$$\begin{cases} A_3 = +(a_{12}\cos\alpha_{23}\sin\alpha_{34} + a_{34}\sin\alpha_{12}) \\ B_3 = -(R_2\sin\alpha_{12}\cos\alpha_{23}\sin\alpha_{34} + R_3\sin\alpha_{12}\sin\alpha_{34}) \\ C_3 = +(a_{23}\cos\alpha_{12}\sin\alpha_{34} + a_{34}\sin\alpha_{23}) \\ D_3 = -(R_2\cos\alpha_{12}\sin\alpha_{23}\sin\alpha_{34} + R_1\sin\alpha_{23}\cos\alpha_{34}) \\ E_3 = +R_2\sin\alpha_{12}\sin\alpha_{23} \\ F_3 = +(a_{12}\sin\alpha_{23}\cos\alpha_{34} + a_{23}\sin\alpha_{12}) \\ G_3 = +(a_{23}\sin\alpha_{12}\cos\alpha_{34} + a_{12}\sin\alpha_{23}) \\ H_3 = -R_2\sin\alpha_{12}\sin\alpha_{23}\cos\alpha_{34} \\ I_3 = +R_1(\cos\alpha_{12}\cos\alpha_{23} + \cos\alpha_{34}) \\ \qquad + R_2(1 + \cos\alpha_{12}\cos\alpha_{23}\cos\alpha_{34}) \\ \qquad + R_3(\cos\alpha_{23} + \cos\alpha_{12}\cos\alpha_{34}) \end{cases} \tag{24}$$

Because not all of the entries in the transformation matrix in Eq. (6) are included in the derivation process, the above results only demonstrate the necessary conditions for the closure relationship among the revolute variables. To ensure the closure, Eqs. (13*a*), (21), and (22) have been taken into the transformation matrix to check whether Eq. (5) is held for the general geometric parameters. In such a way, two sets of solutions to the closure equations are obtained to achieve different linkage closures as follows:

$$\begin{cases} \theta_2 = 2\tan^{-1}\left(\dfrac{-Bterm_2 + \sqrt{Bterm_2^2 - 4Aterm_2 \cdot Cterm_2}}{2Aterm_2}\right) \\ \theta_3 = 2\tan^{-1}\left(\dfrac{-Bterm_3 - \sqrt{Bterm_3^2 - 4Aterm_3 \cdot Cterm_3}}{2Aterm_3}\right) \\ \theta_4 = \theta_1 \\ \theta_5 = \theta_2 \\ \theta_6 = \theta_3 \end{cases} \tag{25}$$

and

$$\begin{cases} \theta_2 = 2\tan^{-1}\left(\dfrac{-Bterm_2 - \sqrt{Bterm_2^2 - 4Aterm_2 \cdot Cterm_2}}{2Aterm_2}\right) \\ \theta_3 = 2\tan^{-1}\left(\dfrac{-Bterm_3 + \sqrt{Bterm_3^2 - 4Aterm_3 \cdot Cterm_3}}{2Aterm_3}\right) \\ \theta_4 = \theta_1 \\ \theta_5 = \theta_2 \\ \theta_6 = \theta_3 \end{cases} \tag{26}$$

Results shown in Eqs. (25) and (26) indicate that there are two distinct forms of the *original* general line-symmetric Bricard 6*R* linkage, both with the property of line-symmetry, named as *Form I linkage* and *Form II linkage*, respectively. Their kinematic paths are plotted in Figs. 2 and 3. Their spatial configurations are

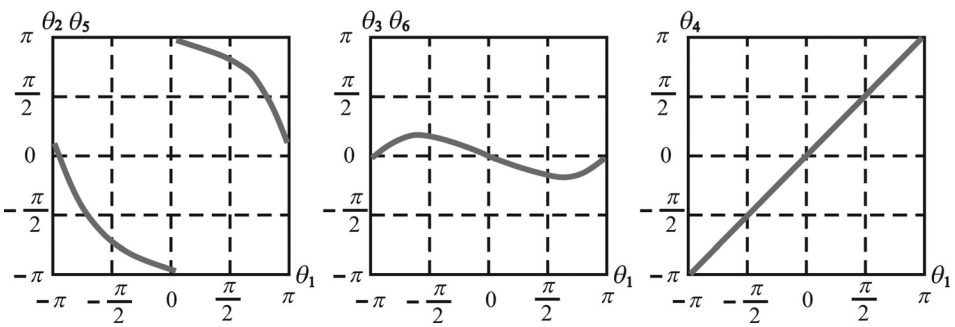

Fig. 3 The kinematic paths of the original Form II general line-symmetric Bricard 6*R* linkage

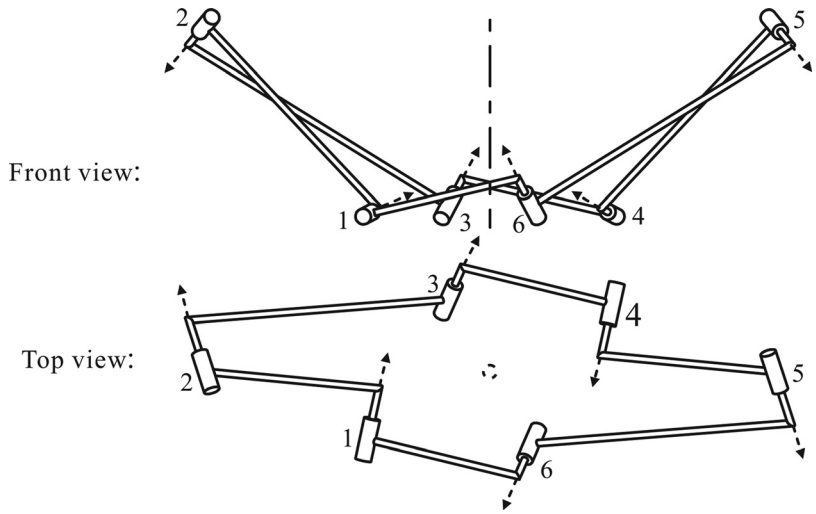

Fig. 4 The spatial configuration of the original Form I general line-symmetric Bricard 6*R* linkage when $\theta_1^{\mathrm{I}} = \pi/3$

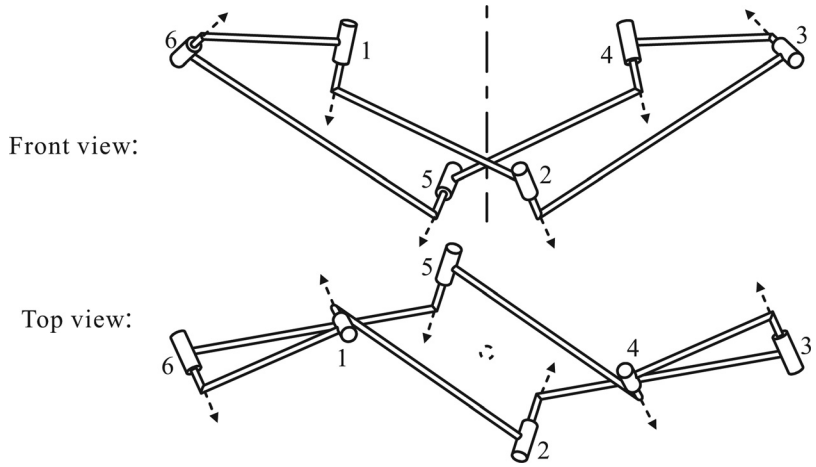

Fig. 5 The spatial configuration of the original Form II general line-symmetric Bricard 6*R* linkage when $\theta_1^{\mathrm{II}} = \pi/3$

illustrated in Figs. 4 and 5, in which the lines of symmetry are identified as the central lines in front views and dashed circles in top views. The geometry parameters of the original general line-symmetric Bricard linkages in Figs. 2–5 are set as

$$a_{12,45} = 2.40, \quad a_{23,56} = 2.90, \quad a_{34,61} = 1.50 \tag{27a}$$

$$\alpha_{12,45} = 4\pi/18, \quad \alpha_{23,56} = 8\pi/18, \quad \alpha_{34,61} = 13\pi/18 \tag{27b}$$

$$R_{1,4} = 0.50, \quad R_{2,5} = 0.55, \quad R_{3,6} = 0.42 \tag{27c}$$

The singularity behaviours of these two linkage forms are examined with the singular value decomposition method, which is a numerical method to solve the singular values of the linkage's Jacobian matrix [30,31]. It is found that these two kinematic paths are solely existed without any bifurcation points, see Fig. 6. Therefore, from Figs. 2, 3, and 6, we can conclude that these two linkage forms are independent with no common configurations under the same geometry conditions.

2.2 Negative Relationship: $\theta_i = -\theta_{i+3}$. For the case of negative relationship, the revolute variables do not follow the line-symmetry property. We can follow the same procedure as the positive relationship to derive the solutions to the closure equations. However, when substituting the results into the transformation matrix, the closure condition in Eq. (5) is not held. Thus, no closed linkage could be achieved with $\theta_i = -\theta_{i+3}$, which means the negative relationship of $\theta_i = -\theta_{i+3}$ is untrue for the original general line-symmetric Bricard linkage.

3 The Solutions of Closure Equations of the Revised General Line-Symmetric Bricard Linkage

The simplified geometry conditions of the revised general line-symmetric Bricard linkage are

$$a'_{i(i+1)} = a'_{(i+3)(i+4)}, \quad \alpha'_{i(i+1)} = \alpha'_{(i+3)(i+4)}$$
$$R'_i = -R'_{(i+3)} (i = 1, 2, 3) \tag{28}$$

The only difference between the geometry conditions of the original and revised linkages is the offset conditions. And entry (1, 1) is in the rotational matrix. Thus, Eq. (7) applies for both the original and revised linkages. Therefore, Eqs. (13*a*) and (13*b*) also can be obtained for the revised general line-symmetric Bricard linkage.

3.1 Positive Relationship: $\theta'_i = \theta'_{i+3}$. For the case of positive relationship, the revolute variables follow the line-symmetry

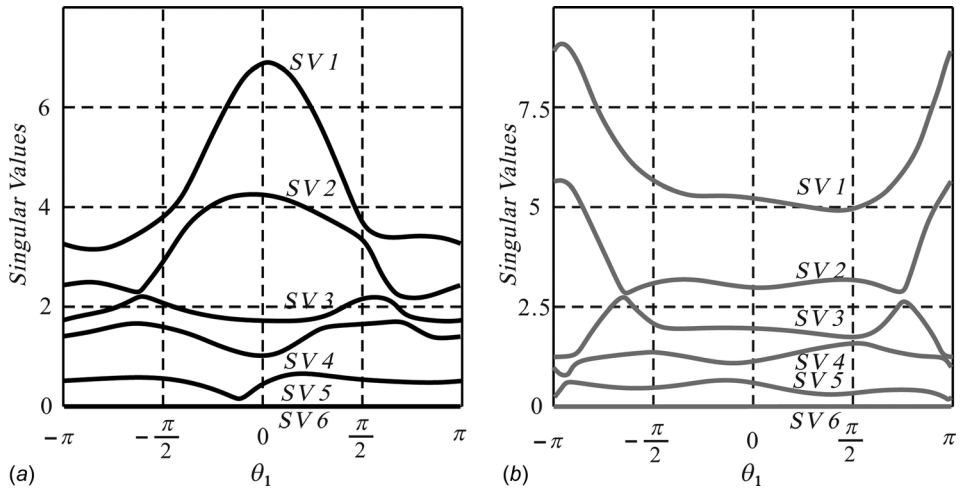

Fig. 6 The SVD results of the original general line-symmetric Bricard 6*R* linkages: (*a*) Form I linkage and (*b*) Form II linkage

property. We can follow the same procedure as Sec. 2.1 to derive the solutions to the closure equations. However, when substituting the result into the transformation matrix, the closure condition in Eq. (5) is not held. Thus, no closed linkage could be achieved with $\theta'_i = \theta'_{i+3}$, which means the positive relationship of $\theta'_i = \theta'_{i+3}$ is untrue for the revised general line-symmetric Bricard linkage.

3.2 Negative Relationship: $\theta'_i = -\theta'_{i+3}$. The same procedure could be carried out to derive the solutions of closure equations for the case of negative relationship. As a result, the following two sets of solutions to the closure equations are concluded to produce two different linkage closures, which are named as the Form I′ and Form II′ of the revised general line-symmetric Bricard linkages:

$$\begin{cases} \theta'_2 = 2\tan^{-1}\left(\dfrac{-Bterm'_2 + \sqrt{Bterm'^2_2 - 4Aterm'_2 \cdot Cterm'_2}}{2Aterm'_2}\right) \\ \theta'_3 = 2\tan^{-1}\left(\dfrac{-Bterm'_3 - \sqrt{Bterm'^2_3 - 4Aterm'_2 \cdot Cterm'_3}}{2Aterm'_3}\right) \\ \theta'_4 = -\theta'_1 \\ \theta'_5 = -\theta'_2 \\ \theta'_6 = -\theta'_3 \end{cases} \tag{29}$$

and

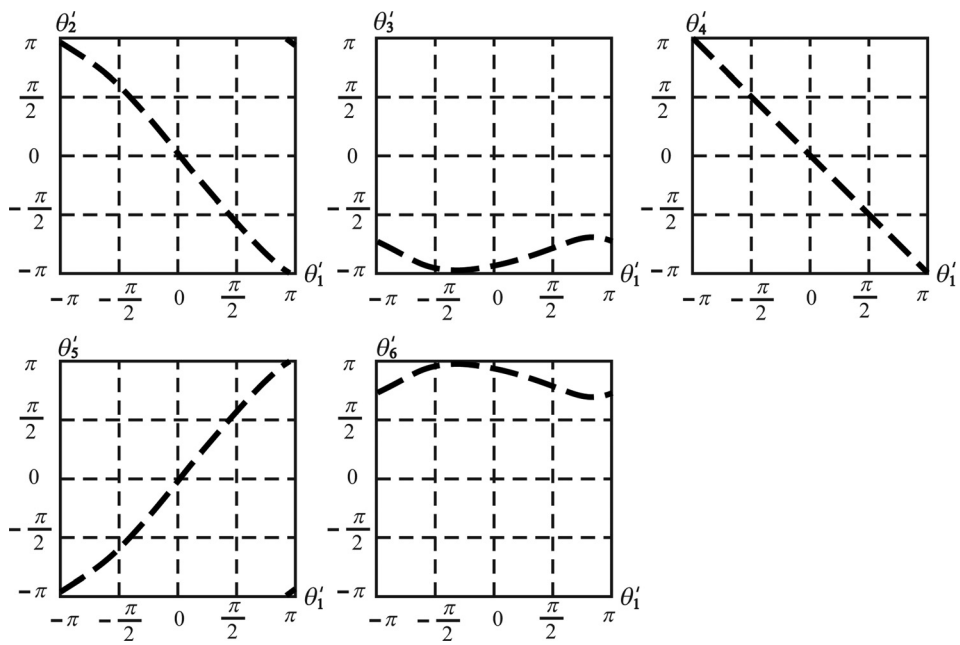

Fig. 7 The kinematic paths of the revised Form I′ general line-symmetric Bricard linkage

$$\begin{cases} \theta'_2 = 2\tan^{-1}\left(\dfrac{-Bterm'_2 - \sqrt{Bterm'^2_2 - 4Aterm'_2 \cdot Cterm'_2}}{2Aterm'_2}\right) \\ \theta'_3 = 2\tan^{-1}\left(\dfrac{-Bterm'_3 + \sqrt{Bterm'^2_3 - 4Aterm'_2 \cdot Cterm'_3}}{2Aterm'_3}\right) \\ \theta'_4 = -\theta'_1 \\ \theta'_5 = -\theta'_2 \\ \theta'_6 = -\theta'_3 \end{cases} \tag{30}$$

where

$$\begin{cases} Aterm'_2 = (A'_2 \sin\theta'_1 + B'_2 \cos\theta'_1 + L'_2) \\ \qquad -(D'_2 + F'_2 \sin\theta'_1 + H'_2 \cos\theta'_1) \\ Bterm'_2 = 2(C'_2 + E'_2 \sin\theta'_1 + G'_2 \cos\theta'_1) \\ Cterm'_2 = (A'_2 \sin\theta'_1 + B'_2 \cos\theta'_1 + L'_2) \\ \qquad +(D'_2 + F'_2 \sin\theta'_1 + H'_2 \cos\theta'_1) \end{cases} \tag{31}$$

$$\begin{cases} A'_2 = +(a'_{34}\sin\alpha'_{12}\cos\alpha'_{23} - a'_{12}\sin\alpha'_{34}) \\ B'_2 = +(R'_3\sin\alpha'_{12}\cos\alpha'_{23}\sin\alpha'_{34} + R_2\sin\alpha'_{12}\sin\alpha'_{34}) \\ C'_2 = -(a'_{23}\sin\alpha'_{12}\cos\alpha'_{34} - a'_{12}\sin\alpha'_{23}) \\ D'_2 = +(R_3\sin\alpha'_{12}\sin\alpha'_{23}\cos\alpha'_{34} - R'_1\sin\alpha'_{12}\sin\alpha'_{23}) \\ E'_2 = -R'_3\sin\alpha'_{23}\sin\alpha'_{34} \\ F'_2 = +(a'_{34}\cos\alpha'_{12}\sin\alpha'_{23} - a'_{23}\sin\alpha'_{34}) \\ G'_2 = -(a'_{23}\cos\alpha'_{12}\sin\alpha'_{34} - a'_{34}\sin\alpha'_{23}) \\ H'_2 = +R'_3\cos\alpha'_{12}\sin\alpha'_{23}\sin\alpha'_{34} \\ L'_2 = +R'_1(\cos\alpha'_{12}\cos\alpha'_{23} - \cos\alpha'_{34}) \\ \qquad +R'_2(\cos\alpha'_{23} - \cos\alpha'_{12}\cos\alpha'_{34}) \\ \qquad +R'_3(1 - \cos\alpha'_{12}\cos\alpha'_{23}\cos\alpha'_{34}) \end{cases} \tag{32}$$

and

$$\begin{cases} Aterm'_3 = (A'_3 \sin\theta'_1 + B'_3 \cos\theta'_1 + L'_3) \\ \qquad -(D'_3 + F'_3 \sin\theta'_1 + H'_3 \cos\theta'_1) \\ Bterm'_3 = 2(C'_3 + E'_3 \sin\theta'_1 + G'_3 \cos\theta'_1) \\ Cterm'_3 = (A'_3 \sin\theta'_1 + B'_3 \cos\theta'_1 + L'_3) \\ \qquad +(D'_3 + F'_3 \sin\theta'_1 + H'_3 \cos\theta'_1) \end{cases} \tag{33}$$

$$\begin{cases} A'_3 = -(a'_{12}\cos\alpha'_{23}\sin\alpha'_{34} - a'_{34}\sin\alpha'_{12}) \\ B'_3 = +(R'_2\sin\alpha'_{12}\cos\alpha'_{23}\sin\alpha'_{34} + R'_3\sin\alpha'_{12}\sin\alpha'_{34}) \\ C'_3 = -(a'_{23}\cos\alpha'_{12}\sin\alpha'_{34} - a'_{34}\sin\alpha'_{23}) \\ D'_3 = +(R'_2\cos\alpha'_{12}\sin\alpha'_{23}\sin\alpha'_{34} + R'_1\sin\alpha'_{23}\sin\alpha'_{34}) \\ E'_3 = +R'_2\sin\alpha'_{12}\sin\alpha'_{23} \\ F'_3 = -(a'_{12}\sin\alpha'_{23}\cos\alpha'_{34} - a'_{23}\sin\alpha'_{12}) \\ G'_3 = -(a'_{23}\sin\alpha'_{12}\cos\alpha'_{34} - a'_{12}\sin\alpha'_{23}) \\ H'_3 = +R'_2\sin\alpha'_{12}\sin\alpha'_{23}\cos\alpha'_{34} \\ L'_3 = +R'_1(\cos\alpha'_{12} - \cos\alpha'_{23}\cos\alpha'_{34}) \\ \qquad +R'_2(1 - \cos\alpha'_{12}\cos\alpha'_{23}\cos\alpha'_{34}) \\ \qquad +R'_3(\cos\alpha'_{23} - \cos\alpha'_{12}\cos\alpha'_{34}) \end{cases} \tag{34}$$

The following geometry conditions are used to plot the kinematic paths in Figs. 7 and 8 using Eqs. (29) and (30), respectively. The spatial configurations of these two linkage forms are plotted in Figs. 9 and 10, respectively. Note that the twists on links 34 and 61 in Eq. (27) differ from the twists on links $3'4'$ and $6'1'$ in Eq. (35) by π. And the offsets are negatively equaled in Eq. (35*c*)

$$a'_{12,45} = 2.40, \quad a'_{23,56} = 2.90, \quad a'_{34,61} = 1.50 \tag{35a}$$

$$\alpha'_{12,45} = 4\pi/18, \quad \alpha'_{23,56} = 8\pi/18, \quad \alpha'_{34,61} = -5\pi/18 \tag{35b}$$

$$R'_1 = -R'_4 = 0.50, \quad R'_2 = -R'_5 = 0.55, \quad R'_3 = -R'_6 = 0.42 \tag{35c}$$

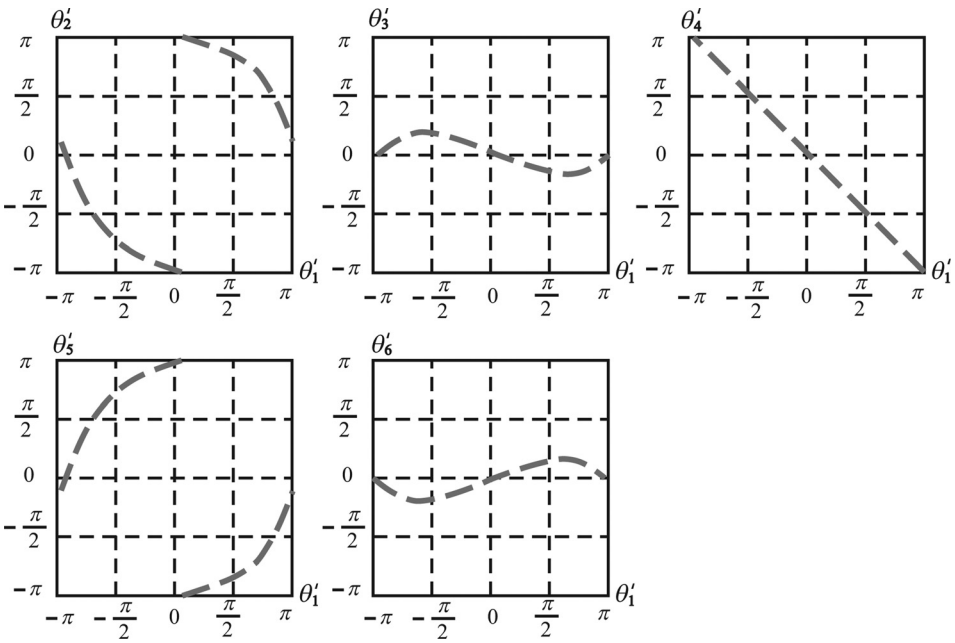

Fig. 8 The kinematic paths of the revised Form II′ general line-symmetric Bricard 6*R* linkage

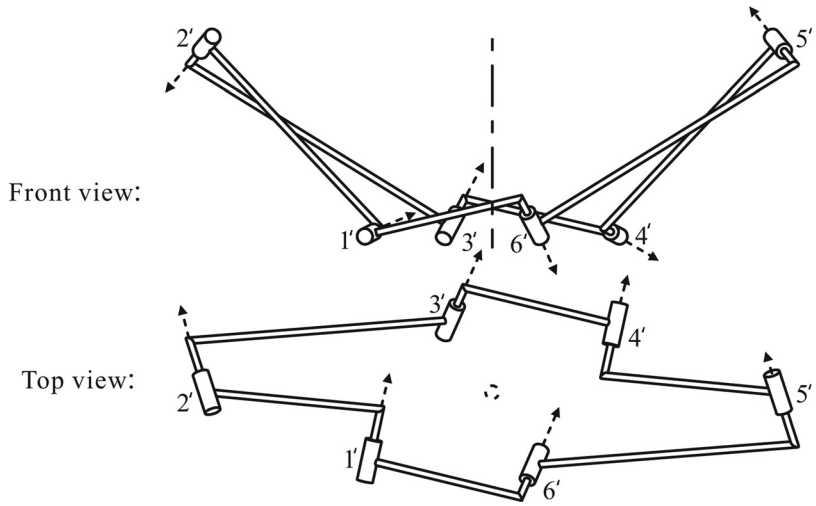

Fig. 9 The spatial configuration of the revised Form I′ general line-symmetric Bricard 6*R* linkage when $\theta_1^{I'} = \pi/3$

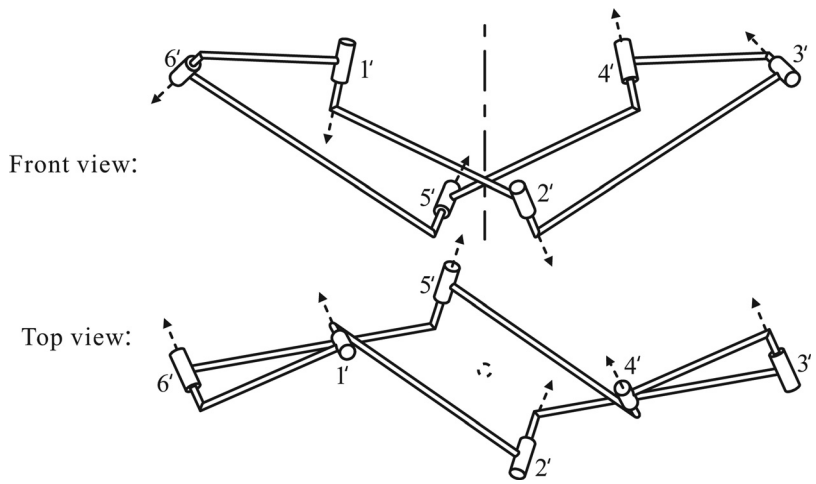

Fig. 10 The spatial configuration of the revised Form II′ general line-symmetric Bricard 6*R* linkage when $\theta_1^{II'} = \pi/3$

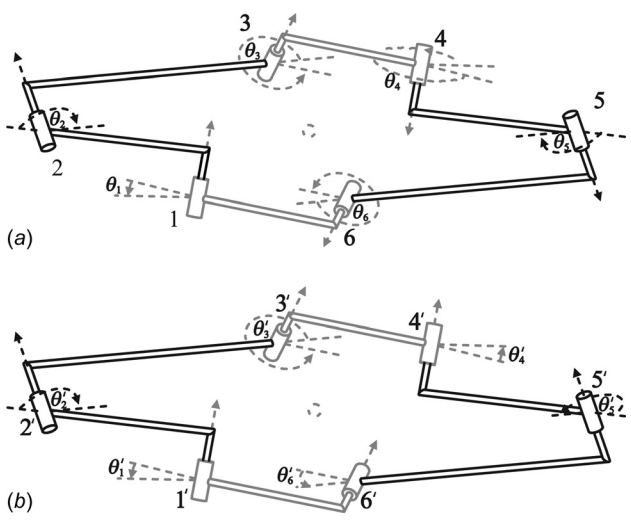

Fig. 11 The illustrations of the general line-symmetric Bricard linkage: (*a*) the original Form I linkage and (*b*) the revised Form I′ linkage

4 Relationship Between the Original and Revised General Line-Symmetric Bricard Linkages

By comparing the solutions of closure equations of the original general line-symmetric Bricard linkage in Eqs. (25) and (26) with the revised general line-symmetric Bricard linkage's in Eqs. (29) and (30), it can be found that when

$$\begin{aligned} &a_{12} = a'_{12} = a_{45} = a'_{45}, \quad a_{23} = a'_{23} = a_{56} = a'_{56}, \\ &a_{34} = a'_{34} = a_{61} = a'_{61} \\ &\alpha_{12} = \alpha'_{12} = \alpha_{45} = \alpha'_{45}, \quad \alpha_{23} = \alpha'_{23} = \alpha_{56} = \alpha'_{56}, \\ &\alpha_{34} = \alpha'_{34} \pm \pi = \alpha_{61} = \alpha'_{61} \pm \pi \\ &R_1 = R'_1 = R_4 = -R'_4, \quad R_2 = R'_2 = R_5 = -R'_5, \\ &R_3 = R'_3 = R_6 = -R'_6 \end{aligned} \tag{36}$$

we will have

$$\begin{aligned} &\theta_1 = \theta'_1, \quad \theta_2 = \theta'_2, \quad \theta_3 = \theta'_3, \quad \theta_4 = -\theta'_4, \quad \theta_5 = -\theta'_5, \\ &\theta_6 = -\theta'_6 \end{aligned} \tag{37}$$

for both linkage forms, which has been confirmed by the kinematic paths in Figs. 2, 3, 7, and 8. Even though the geometry

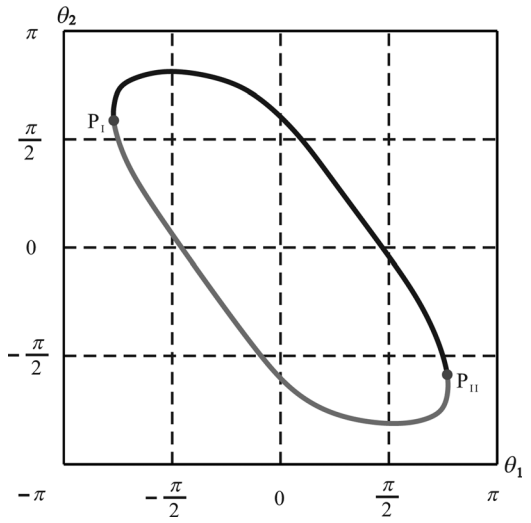

Fig. 12 The kinematic paths of the general line-symmetric octahedral Bricard linkage. Here, the geometric parameters are the same as Eq. (27) with $a_{i(i+1)} = 0$. The black solid line is from the closure equations of the Form I linkage; the grey solid line is from those of the Form II linkage.

conditions and revolute variables in the revised general line-symmetric Bricard linkage are not line-symmetric, the spatial configurations of the resultant linkages in Figs. 9 and 10 are still in a line-symmetric manner.

In fact, with the geometric parameters in Eqs. (27) and (35) which satisfies Eq. (36), the spatial configurations of the revised Forms I′ and II′ linkages in Figs. 9 and 10 are the same as those of the original Forms I and II linkages' in Figs. 4 and 5. Take the Form I of the original and revised general line-symmetric Bricard linkages, for example, the joints 4, 5, 6 in Figs. 11(*a*) and 11(*b*) are in opposite directions due to $a_{34} = a'_{34} \pm \pi = a_{61} = a'_{61} \pm \pi$. As a result, $\theta_4 = -\theta'_4$, $\theta_5 = -\theta'_5$, $\theta_6 = -\theta'_6$. The same analysis could be carried out for the relationship between the Form II original and revised linkages. The original and revised linkages are actually equivalent to each other with different setups on joint axis directions.

5 Conclusion and Discussions

In this paper, the kinematics of the original general line-symmetric Bricard 6*R* linkage is investigated through the algebraic derivation of the solutions to the closure equations. It is found that there are two independent linkage forms, which are called the Form I linkage and Form II linkage, under the same geometry conditions. The revised general line-symmetric Bricard linkage is also investigated with negatively equaled offsets on the opposite joints. Further analysis shows that the original and revised linkages are equivalent with different setups on the joint axis directions. Results in this paper offer an in-depth understanding about the kinematics of the general line-symmetric Bricard linkage.

For the general line-symmetric octahedral Bricard linkage as a special case of the general line-symmetric Bricard linkage, we can substitute $a_{i(i+1)} = 0 (i = 1, 2, \ldots, 6)$ into the two sets of closure equations of the general line-symmetric Bricard linkage to give the closure equations of the line-symmetric octahedral Bricard linkage. As shown in Fig. 12, it is found that the closure equations of each linkage form can only produce half of the kinematic paths of the line-symmetric octahedral Bricard linkage, which then join together at points P_I and P_{II} to form a full-cycle motion of the linkage. When the revolute variables are in negative relationship, no closure can be achieved for the line-symmetric octahedral Bricard linkage. The results shown in Fig. 12 comply with previous results in Refs. [8,9].

It should be pointed out that since the quadratic equation is used in the process to solve the closure equations, its discriminant must be non-negative in order to obtain the valid solution. For example, the discriminant of Eq. (19) must follow the condition to ensure a valid input–output relationship between θ_1 and θ_2

$$Bterm_2^2 - 4Aterm_2 \cdot Cterm_2 \geq 0 \tag{38}$$

and for the relationship between θ_1 and θ_3

$$Bterm_3^2 - 4Aterm_3 \cdot Cterm_3 \geq 0 \tag{39}$$

must hold. Equations (38) and (39) contain only the input kinematic variable θ_1 and the geometric parameters of the linkage, $a_{i(i+1)}, \alpha_{i(i+1)}$, and R_i. Then the combinations of their solutions for the range of θ_1 in the terms of $a_{i(i+1)}, \alpha_{i(i+1)}$, and R_i offer the valid linkage closure between input kinematic variable θ_1 and the output kinematic variables $\theta_{2,3,4,5,6}$, which is established in Eqs. (25) and (26). So with the given geometric parameters of the linkage, the valid input kinematic variable can be determined by Eqs. (38) and (39). In general, the line-symmetric Bricard linkage in Figs. 2, 3, 7, and 8, $\theta_1 \in [-\pi, \pi)$, and the special line-symmetric octahedral Bricard linkage in Fig. 12, the domain of the definition for θ_1 is $[-2.4816, 2.4914)$.

Acknowledgment

C.-Y. Song would like to thank Nanyang Technological University, Singapore, for providing the University Graduate Scholarship during his PhD study. Special thanks to Dr. Coutsias for his translation of the original work of Bricard from French to English [32]. With his volunteering and excellent work, Bricard's outstanding work can be reached with wider popularity. Y. Chen would like to thank the financial support from the National Natural Science Foundation of China (Projects No. 51275334 and No. 51290293) and Tianjin Municipal Science and Technology Development Program (Grant 13JCZDJC26400).

Nomenclature

$A, B, \ldots, H$, and L = the symbols of simplified mathematical relationships

$a_{i(i+1)}$ = the length of link $i(i+1)$, which is the common normal distance from z_i to z_{i+1} positively about x_i, and defined in the range of $(-\infty, +\infty)$

Aterm, *Bterm*, and *Cterm* = the symbols of simplified mathematical relationships

$\mathbf{d}_{3\times1}$ = the 3×1 translational vector

Forms I, II = the different linkage closures

$\mathbf{I}$ = the identity matrix

R_i = the offset of joint i, which is the common normal distance from x_i to x_{i+1} positively along z_i, and defined in the range of $(-\infty, +\infty)$

$\mathbf{R}_{3\times3}$ = the 3×3 rotational matrix

$\mathbf{T}_{i(i+1)}$ = the transformation matrix from joint i to joint $i+1$

x and x' = the corresponding parameters in two types of general line-symmetric Bricard linkage, where x is for the parameters in the *original* linkage and x' is for the parameters in the *revised* linkage

x_i = the coordinate axis along the common normal between joint axes from joint i to joint $i+1$

z_i = the coordinate axis along the revolute axis of joints i

$\alpha_{i(i+1)}$ = the twist of link $i(i+1)$, which is the rotation angle from z_i to z_{i+1} positively about x_i, and defined in the range of $[-\pi, \pi)$

θ_i = the revolute variable of joint i, which is the rotation angle from x_i to x_{i+1} positively about z_i, and defined in the range of $[-\pi, \pi)$

References

[1] Bricard, R., 1897, "Mémoire sur la théorie de l'octaèdre articulé," J. Pure Appl. Math., **3**, pp. 113–150.

[2] Bricard, R., 1927, *Leçons de cinématique*, Gauthier-Villars, Paris.

[3] Baker, J. E., 1980, "An Analysis of the Bricard Linkages," Mech. Mach. Theory, **15**(4), pp. 267–286.

[4] Phillips, J., 1984, *Freedom in Machinery I: Introducing Screw Theory*, Cambridge University Press, Cambridge, UK.

[5] Phillips, J., 1990, *Freedom in Machinery II: Screw Theory Exemplified*, Cambridge University Press, Cambridge, UK.

[6] Bennett, G. T., 1911, "Deformable Octahedra," Proc. London Math. Soc., **2**(10), pp. 309–343.

[7] Baker, J. E., 1986, "Limiting Positions of a Bricard Linkage and Their Possible Relevance to the Cyclohexane Molecule," Mech. Mach. Theory, **21**(3), pp. 253–260.

[8] Lee, C. C., 1996, "On the Generation Synthesis of Movable Octahedral 6*R* Mechanisms," ASME Design Engineering Technical Conferences and Computers in Engineering Conference, Irvine, CA, August 18–22, ASME Paper No. 96-DETC/MECH-1576.

[9] Chai, W. H., and Chen, Y., 2010, "The Line-Symmetric Octahedral Bricard Linkage and Its Structural Closure," Mech. Mach. Theory, **45**(5), pp. 772–779.

[10] Husty, M. L., and Karger, A., 1996, "On Self-Motions of a Class of Parallel Manipulators," *Advances in Robot Kinematics*, J. Lenarcic and V. Parenti-Castelli, eds., Kluwer Academic Publishers, Dordrecht, Netherlands, pp. 339–348.

[11] Husty, M. L., 2000, "E. Borel's and R. Bricard's Papers on Displacements With Spherical Paths and Their Relevance to Self-Motions of Parallel Manipulators," International Symposium on History of Machines and Mechanisms (HMM 2000), M. Ceccarelli, ed., Kluwer Academic Publisher, Dordrecht, Netherlands, pp. 163–172.

[12] Husty, M. L., and Zsombor-Murray, J., 1994, "A Special Type of Singular Stewart-Gough Platform," *Advances in Robot Kinematics*, J. Lenarcic and B. Ravani, eds., Springer, Dordrecht, Netherlands, pp. 449–458.

[13] Nawratil, G., 2011, "Self-Motions of TSSM Manipulators With Two Parallel Rotary Axes," ASME J. Mech. Robot., **3**(3), p. 031007.

[14] Nawratil, G., 2010, "Flexible Octahedra in the Projective Extension of the Euclidean 3-Space," J. Geometry Graphics, **14**(2), pp. 147–169.

[15] Nelson, G. D., 2010, "Extending Bricard Octahedra," arXiv:1011.5193v1. Available at: http://arxiv.org/ftp/arxiv/papers/1011/1011.5193.pdf

[16] Goldberg, M., 1974, "A 6-Plate Linkage in Three Dimensions," Math. Gazette, **58**, pp. 287–289.

[17] Yu, H. C., 1981, "The Deformable Hexahedron of Bricard," Mech. Mach. Theory, **16**(6), pp. 621–629.

[18] Wohlhart, K., 1993, "The Two Types of the Orthogonal Bricard Linkage," Mech. Mach. Theory, **28**(6), pp. 809–817.

[19] Baker, J. E., and Wohlhart, K., 1994, "On the Single Screw Reciprocal to the General Line-Symmetric Six-Screw Linkage," Mech. Mach. Theory, **29**(1), pp. 169–175.

[20] Baker, J. E., 1997, "The Single Screw Reciprocal to the General Plane-Symmetric Six-Screw Linkage," J. Geometry Graphics, **1**(1), pp. 5–12.

[21] Lee, C. C., 2000, "Computational and Geometric Investigation on the Reciprocal Screw Axis of Bricard Six-Revolute Mechanisms," ASME Design Engineering Technical Conference and Computers and Information in Engineering Conference (DETC'00), Baltimore, MD, September 10–13, ASME Paper No. DET00/MECH-6104, pp. 93–101.

[22] Chen, Y., You, Z., and Tarnai, T., 2005, "Threefold-Symmetric Bricard Linkages for Deployable Structures," Int. J. Solids Struct., **42**(8), pp. 2287–2301.

[23] Chen, Y., and Chai, W. H., 2011, "Bifurcation of a Special Line and Plane Symmetric Bricard Linkage," Mech. Mach. Theory, **46**(4), pp. 515–533.

[24] Lee, C. C., and Yan, H. S., 1993, "Movable Spatial 6*R* Mechanisms With Three Adjacent Parallel Axes," ASME J. Mech. Des., **115**(3), pp. 522–529.

[25] Racila, L., and Dahan, M., 2010, "Spatial Properties of Wohlhart Symmetric Mechanism," Meccanica, **45**(2), pp. 153–165.

[26] Chen, Y., 2003, "Design of Structural Mechanisms," Ph.D. dissertation, University of Oxford, Oxford, UK.

[27] Wohlhart, K., 1987, "A New 6R Space Mechanism," 7th World Congress on the Theory of Machines and Mechanisms, Sevilla, Spain, September 17–22, pp. 193–198.

[28] Denavit, J., and Hartenberg, R. S., 1955, "A Kinematic Notation for Lower-Pair Mechanisms Based on Matrices," ASME J. Appl. Mech., **22**(2), pp. 215–221.

[29] Mavroidis, C., and Roth, B., 1994, "Analysis and Synthesis of Overconstrained Mechanisms," ASME Design Technical Conferences, Minneapolis, MN, September 11–14, pp. 115–133.

[30] Pellegrino, S., 1993, "Structural Computations With the Singular Value Decomposition of the Equilibrium Matrix," Int. J. Solids Struct., **30**(21), pp. 3025–3035.

[31] Gan, W. W., and Pellegrino, S., 2006, "A Numerical Approach to the Kinematic Analysis of Deployable Structures Forming a Closed Loop," Proc. Inst. Mech. Eng. Part C: J. Mech. Eng. Sci., **220**(7), pp. 1045–1056.

[32] Bricard, R., 1897, "Mémoire sur la théorie de l'octaèdre articulé," J. Pure Appl. Math., **3**, pp. 113–150 (English translation by E. A. Coutsias, 2010, e-print, http://arxiv.org/abs/1203.1286).